Mathematics in Applied Sciences and Engineering
Volume **6**, Number **1**, March **2025**, pp.**20-35**
https://ojs.lib.uwo.ca/mase
https://doi.org/10.5206/mase/19995

HEAT TRANSFER IN AN MHD FLOW OF AN ERYING-POWELL FLUID OVER A CONVECTIVELY HEATED STRETCHING SHEET IN THE PRESENCE OF HEAT SOURCE AND THERMAL RADIATION

LATEEF O. SOGBETUN, B. I. OLAJUWON, AND O. FAGBEMIRO

Abstract. This study investigates the effects of viscous dissipation, Joule heating, and a heat source on the magnetohydrodynamic flow of an Eyring-Powell fluid over a convectively heated stretched sheet with convective boundary conditions. The fluid flows over a surface heated by a hot fluid from beneath through convection. The fluid's viscosity follows a Reynolds model, while its thermal conductivity varies linearly with temperature. By applying the standard similarity method, the governing nonlinear partial differential equations are transformed into ordinary differential equations. These equations are then solved numerically using the Spectral Quasi-Linearization Method (SQLM). The study presents and discusses graphical results that highlight the key fluid variables influencing velocity and temperature profiles. The findings of this research could have significant implications for various engineering applications, such as heat exchangers, chemical reactors, and thermal management systems.

1. Introduction

Due to its numerous practical applications, researchers have recently focused more on the investigation of boundary layer flow across a stretching sheet. Empirical studies of fluid behavior over varying surfaces provide vital insight that are highly relevant to manufacturing processes. Industries such as polymer production, lubricant manufacturing, aerodynamic plastic sheet extrusion, liquid coating of photographic films, metallic plate condensation in a cooling bath, and glass manufacturing are among those where fluid flow over stretching surfaces plays a critical role[1]. Crane et al. [11] investigated the boundary layer flow of a viscous fluid across a sheet moving with velocity proportional to the distance of the aperture. Kumari and Nath [20] examined the exact solution of two-dimensional flow over a stretching surface in the presence of a magnetic field. Mukhopadhyay [26] analyzed slip effects on MHD boundary layer flow past an exponentially stretched sheet with suction/blowing in the presence of thermal radiation. Chamkha and Mansour [9] studied the effect of chemical reactions and unsteady free convection on heat transfer over a stretching sheet in a porous medium. Turkyilmazoglu [34] presented a closed-form solution for two-dimensional laminar flow over a continuously stretched sheet. Tawade et al [33] proposed a numerical approach for solving unsteady, two dimensional, laminar nanofluid flow using the 4th-order Runge-Kutta method combined with the shooting method. Ibrahim et al. [16] investigated the stagnation point flow of an MHD nanofluid towards a stretching sheet.

Extensive studies of the Erying-Powell model under various physical conditions have been conducted by numerous researchers.The Eyring-Powell model is one of the non-Newtonian fluid models derived from the kinetic theory of gases rather than an empirical formulas. It also accurately reduces to Newtonian behaviour at both low and high shear rates. The model's significance in industries such

Received by the editors 23 July 2024; accepted 5 March 2025; published online 18 March 2025.
2020 *Mathematics Subject Classification.* 76W05, 76A05, 80A20, 76D10, 76R10.
Key words and phrases. Erying-Powell, viscous dissipation, heat source, joule heating, quasi-linearization method.

as bio-fluid, food processing, and medical applications has motivated extensive research on this fluid [6],[24],[27]. Using a numerical technique, Patel and Timol [23] investigated the flow of the Powell-Eyring model's flow under asymptotic boundary conditions. Hayat et al.[13] studied the influence of thermal radiation on magnetohydrodynamics Eyring Powell fluid flow over a stretching surface using an analytical method. Rosca and Pop [31] analyzed the flow and heat transfer of Powell-Eyring fluid over a shrinking surface in a parallel free stream. Panigrahi et al.[28] explored the analytical solution for the Powell-Erying fluid flow past a nonlinear stretching sheet. Hayat et al. [15] examined the impact of convective boundary conditions on the steady flow of a Powell-Eyring fluid over a moving surface. In a separate study, Hayat et al. [14] investigated the effects of heat flux and chemical reactions on the flow of Eyring-Powell fluid past an exponentially stretching surface. Khader and Babatin [18] numerically solved the problem of the Powell-Eyring fluid flow under the influence of a magnetic field and thermal radiation using the spectral collocation method. Recently, Abbas et al [2] studied magnetohydrodynamic (MHD) dissipative Powe-Erying fluid flow due to a stretching sheet with convective boundary condition and slip. The problem was solved numerically using Runge-Kutta Method combined with the shooting technique. However, the roles of some vital fluid properties, such as thermal radiation, heat generation/absorption and the thermal Grashof number were not included in the model.

Numerous studies have highlighted the significant role of heat sources in influencing the functionality of thermal systems. The temperature difference between a surface and the surrounding fluid is often affected by the presence of heat sources or sinks. Heat generation frequently occurs in combustion processes, such as in engines, boilers, and furnaces, while heat absorption is central to cooling systems like refrigeration, air conditioning, heat exchangers, and more. Heat generation or absorption can vary, being constant, spatially dependent, or temperature-dependent. Chamkha and Khaled [8] investigated heat and mass transfer in natural convection in the presence of heat generation/absorption and a magnetic field. Their findings revealed an increase in the heat transfer rate with higher heat absorption parameters. In another study, Chamkha [10] analyzed the effect of heat absorption on time-dependent magnetohydrodynamic (MHD) flow across a vertical porous plate. He observed that a higher heat absorption parameter reduces the Nusselt number. Asimoni et al. [3] presented an analysis of two-dimensional MHD convective nanofluid flow in a lid-driven cavity, considering the influence of chemical reactions and heat absorption coefficients. Asogwa et al [4] investigated the impact of chemical reactions and heat absorption on the flow of a Casson fluid over a rapidly accelerated inclined Riga plate, considering ramped wall temperature and ramped surface concentration. Flow behavior of thin liquid films on a linear stretching sheet, incorporating the effects of thermocapillary and variable heat generation or absorption was studied by Janthe et al. [17]. Analytical investigation on the influence of heat generation or absorption on mixed convection flow field within a vertical channel containing a porous matrix was reported by Kumar et al. [19]. Manvi et al [23] examined the heat dissipation analysis across a layered stretching sheet, focusing on the magneto-hydrodynamic (MHD) mixed convective flow of an Eyring-Powell fluid.

Radiation plays a pivotal role in thermal distribution, profoundly affecting heat transfer processes and temperature regulation. Its importance is underscored in thermal systems, where the intensity of emitted radiation is directly tied to an object's temperature. Thermal radiation is particularly significant in a wide range of industrial applications, such as energy conversion systems, gas turbines, aerospace technology, chemical engineering, nuclear reactors, metallurgical operations, and renewable energy technologies. A thorough understanding and optimization of thermal radiation effects are critical for developing high-temperature energy conversion systems, including those used in rocket engines,

missile re-entry scenarios, astrophysical phenomena, and heat exchangers. Recent research has extensively explored the behavior and impact of radiation in thermal systems. For example, Khan et al. examined entropy generation in non-Newtonian nanofluids under the influence of radiation. Daniel et al. [12] studied the combined effects of viscous dissipation and thermal radiation on chemically reactive magnetohydrodynamic (MHD) fluids. Rashad [30] investigated how slip conditions and radiation affect MHD flow dynamics. Mittal and Patel [25] analyzed the interplay of nonlinear thermal radiation, Brownian motion, and chemical reactions in two-dimensional MHD stagnation point flow. Lopez et al. [21] explored the role of convective boundary conditions and radiation in MHD nanofluid flow. Sharma [32] developed a simulation to study the effects of radiative heat flux and viscous dissipation in MHD fluid flow. Additionally, Bilal et al [7]. examined the thermal characteristics of hydromagnetic Williamson nanofluid flow, incorporating the influence of radiation. Athal et al. [5] analysed how thermal radiation and chemical reactions jointly impacted on MHD flow of a hyperbolic tangent fluid containing nanoparticles over a stretched surface. A numerical analysis of Casson nanofluids flowing through porous materials on stretched magnetic surfaces, considering non-uniform heat source/sink and radiation was reported by Manvi et al [22].

The literature reviewed indicates that limited research has been conducted on the MHD flow of an Eyring-Powell fluid, particularly toward a convectively heated stretching sheet with convective boundary conditions. The inclusion of slip and convective boundary conditions in the study of Eyring-Powell fluids enhances the model's physical relevance, making it more applicable to real-world problems such as microfluidics, industrial lubrication, thermal management systems and, heat exchangers. These conditions provide a deeper understanding of fluid behavior, heat transfer, and fluid-surface interactions, which are critical for optimizing system performance. Thus, this study aims to advance the mathematical analysis of MHD Eyring-Powell fluid flow through a porous medium with slip conditions, influenced by thermal radiation, heat generation/absorption, thermal Grashof number, viscous dissipation, nonlinear thermal conductivity, and Joule heating. The proposed research has significant applications across various engineering fields, such as heat exchangers, chemical reactors, cooling systems, renewable energy technologies, and thermal management systems. The dimensionless equations are solved numerically using the Spectral Quasi-Linearization Method (SQLM), with computational implementation carried out in MATLAB software. The effects of various dimensionless parameters on temperature and velocity profiles are analyzed and presented graphically.

The key contributions and novelties of this study are summarized as follows:

(i) This research investigates the thermal behavior of MHD Eyring-Powell fluid over a convectively heated stretching sheet with convective boundary conditions—an area that is relatively unexplored in existing literature.
(ii) The model incorporates convective boundary conditions, temperature-dependent viscosity and nonlinear thermal conductivity, offering a more precise representation of heat transfer in fluids.
(iii) The study simultaneously examines the combined influence of viscous dissipation, Joule heating, thermal Grashof number, and a heat source on the MHD flow of an Eyring-Powell fluid over a convectively heated stretching sheet.

2. Model Formulation

Consider an incompressible, two dimensional flow of a non-Newtonian Erying-Powell fluid past a convectively heated linearly stretching sheet. The fluid flow is steady and laminar with the sheet velocity assuming the form $U_w = ax$ where a is a constant. A schematic representation of the model is provided in figure 1. A transverse magnetic field of strength B_0 is applied perpendicular to the fluid layers.

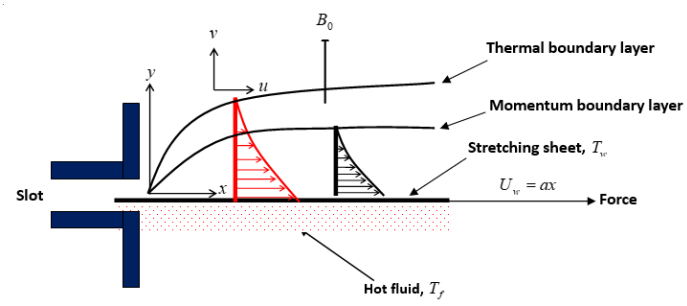

FIGURE 1. Physical configuration of the problem

The stretched sheet surface is being heated by hot fluid from beneath through convection with the temperature $T_f = T_\infty + Ax^m, T_\infty < T_f$, where T_∞ denotes the constant temperature of the cold fluid far away from the sheet, A and m are constants. The effects of thermal variables such as viscous dissipation, thermal radiation, heat source and Joule heating on the fluid properties are incorporated into the analysis.

Using the boundary layer approximation, the simplified continuity equation, momentum equation and energy equation for an incompressible fluid conform with Erying-Powell model are as follows:

$$\frac{\partial u}{\partial x} + \frac{\partial v}{\partial y} = 0 \tag{2.1}$$

$$u\frac{\partial u}{\partial x} + v\frac{\partial u}{\partial y} = \frac{1}{\rho_\infty}\frac{\partial}{\partial y}\left[\mu^x \frac{\partial u}{\partial y} + \frac{1}{\tilde{\beta}C}\frac{\partial u}{\partial y} - \frac{1}{6\tilde{\beta}C^3}\left(\frac{\partial u}{\partial y}\right)^3\right] + g\beta^*(T - T_\infty) - \frac{\sigma\beta^2}{\rho_\infty}u, \tag{2.2}$$

$$\begin{aligned} u\frac{\partial T}{\partial x} + v\frac{\partial T}{\partial y} &= \frac{1}{\rho_\infty c_p}\frac{\partial}{\partial y}\left[k(T)\frac{\partial T}{\partial y}\right] + \frac{\sigma\beta^2}{\rho_\infty c_p}u^2 \\ &+ \frac{1}{\rho_\infty c_p}\left[\mu^*\left(\frac{\partial u}{\partial y}\right)^2 + \frac{1}{\tilde{B}C}\left(\frac{\partial u}{\partial y}\right)^2 - \frac{1}{6\tilde{B}C^3}\left(\frac{\partial u}{\partial y}\right)^4\right] + \frac{Q_0}{\rho_\infty c_p}(T - T_\infty) - \frac{1}{\rho_\infty c_p}\frac{\partial q_r}{\partial y}. \end{aligned} \tag{2.3}$$

The boundary conditions for the continuity, momentum, and energy equations (2.1)-(2.3) are as follows:

$$\begin{aligned} &u = ax + \frac{\lambda_1}{\mu_\infty}\left[\mu^*\frac{\partial u}{\partial y} + \frac{1}{\tilde{\beta}C}\frac{\partial u}{\partial y} - \frac{1}{6\tilde{\beta}C^3}\left(\frac{\partial u}{\partial y}\right)^3\right], \quad v = 0, \\ &-k\left(\frac{\partial T}{\partial y}\right) = h_f(T_f - T_\infty) \text{ at } y = 0, \\ &u \to 0, \quad T \to T_\infty \quad \text{as } y \to \infty. \end{aligned} \tag{2.4}$$

Here, u and v denote the velocity components along the x and y axes, T is symbol for temperature of the fluid ρ_∞ stands for the ambient fluid density, σ connotes electricity conductivity parameter, c_p represents the specific heat term, $k(T)$ signifies nonlinear thermal conductivity, μ is the dynamic viscosity, $\tilde{\beta}$ and C stand for the Powell-Eyring fluid parameters.

The fluid viscosity follows a Reynolds model and the thermal conductivity is a linear function of temperature and given as:

$$\mu^* = \mu_\infty e^{-\gamma\theta} \text{ and } k(T) = k_\infty(1 + \delta^*(T - T_\infty)) \tag{2.5}$$

where γ^* is a viscosity variation parameter and μ_∞ is the fluid dynamic viscosity at the ambient temperature, k_∞ is the constant value of the coefficient of thermal conductivity far from the plate, and δ^* is a small parameter.

Introducing the following stream function and similarity variables in (2.6)

$$\psi = \sqrt{av_\infty} x f(\eta), \quad \eta = \sqrt{\frac{a}{v_\infty}} y, \quad \theta(\eta) = \frac{T - T\infty}{T_f - T_\infty}, \tag{2.6}$$

Equations (2.1) - (2.4) become

$$f'''\left(e^{-\gamma\theta} + \alpha\left(1 - \delta f''^2\right)\right) - \gamma f'' e^{-\gamma\theta}\theta' - f'^2 + ff'' - Mf' + G_{rx}\theta = 0, \tag{2.7}$$

$$\begin{aligned}\frac{1}{Pr}\left(\left(1+\epsilon\theta\right)\theta'' + \epsilon\theta'^2\right) + f\theta' - 2f'\theta + Ecf''^2\left(\left(e^{-\gamma\theta}+\alpha\right) - \frac{\alpha\delta}{3}f''^2\right) + Q\theta \\ + MEcf'^2 + \frac{1}{Pr}R_d\theta'' = 0,\end{aligned} \tag{2.8}$$

$$\begin{cases} f(0) = 0 \qquad f'(0) = 1 + \lambda e^{-\gamma\theta} f''(0) + \lambda\alpha f''(0) - \dfrac{1}{3}\lambda\alpha\delta f''^3(0), \\ \theta'(0) = -\Delta\dfrac{(1-\theta(0))}{(1+\epsilon\theta(0))} \quad \text{at} \quad \eta = 0, \end{cases} \tag{2.9}$$

$$f'(\eta) \to 0, \qquad \theta(\eta) \to 0 \qquad \text{as } \eta \to \infty. \tag{2.10}$$

Here a prime denotes differentiation with respect to η. The quantities α and δ connote the material fluid parameters, λ represents the slip parameter, M signifies the magnetic parameter, G_{rx} is thermal grashof number, Δ stands for the surface-convection parameter, Q denotes heat source, Ec signifies the Eckert number, Pr connotes the Prandtl number and ϵ symbolizes thermal conductivity parameter. These quantities are mathematical represented as follows:

$$\alpha = \frac{1}{\tilde{\beta}C\mu_\infty}, \qquad \delta = \frac{aU_w^2}{2v_\infty C^2}, \qquad G_{rx} = \frac{g\beta^8(T_f - T_\infty)}{a^2 x}, \qquad Pr = \frac{c_p\mu_\infty}{k_\infty},$$
$$\epsilon = \delta^*(T_f - T_\infty), \qquad Ec = \frac{U_w^2}{c_p(T_f - T_\infty)}, \qquad M = \frac{\sigma B^2}{\rho_\infty a}, \qquad Q = \frac{Q_0}{\rho_\infty c_p a},$$
$$R_d = \frac{16\sigma^* T_\infty^3}{3k^* k_\infty}, \qquad \Delta = \frac{h_f}{k_\infty}\sqrt{\frac{v_\infty}{a}}, \qquad \lambda = \lambda_1\sqrt{\frac{a}{v_\infty}}.$$

The surface drag force and Nusselt number are expressed as follows:

$$Cf = \frac{\tau_w}{\rho(U_w)^2}, \qquad Nu_x = \frac{xq_w}{K_\infty(T_f - T_\infty)}, \tag{2.11}$$

where the wall shear stress τ_w and wall heat flux q_w are defined as

$$\tau_{ij} = -\left[\mu^*\frac{\partial u}{\partial y} + \frac{1}{\tilde{\beta}}sinh^{-1}\left(\frac{1}{C}\frac{\partial u}{\partial y}\right)\right]_{y=0} = -\left[\mu^*\frac{\partial u}{\partial y} + \frac{1}{\tilde{\beta}C}\frac{\partial u}{\partial y} - \frac{1}{6\beta\tilde{C}^3}\left(\frac{\partial u}{\partial y}\right)^3\right]_{y=0}, \tag{2.12}$$

$$q_w = \left(-k(T)\frac{\partial T}{\partial y} + q_z\right)_{y=0}. \tag{2.13}$$

Using equations (2.6), (2.12) and (2.13) in (2.11), we have

$$CfRe_x^{\frac{1}{2}} = -\left[\left(e^{-\gamma\theta(0)} + \alpha\right)f''(0) - \frac{\alpha\delta}{3}f''^3(0)\right], \tag{2.14}$$

$$Nu_x Re_x^{-\frac{1}{2}} = -(1 + \epsilon\theta(0) + R_d)\theta'(0). \tag{2.15}$$

where $Re_x = U_w x/v_\infty$.

3. Method of Solution

The suitable initial solutions for equations (2.7)–(2.8) subject to the boundary conditions in equation (2.9)-(2.10) are

$$f_r = \left(\frac{1}{3}\lambda\alpha\delta - \lambda e^{-\gamma\theta} - \lambda\alpha - 2\right)\eta e^{-\eta} + \left(\frac{2}{3}\lambda\alpha\delta - 2\lambda e^{-\gamma\theta} - 2\lambda\alpha - 3\right)e^{-\eta} + 2\lambda e^{-\gamma\theta} + 2\lambda\alpha - \frac{2}{3}\lambda\alpha\delta + 3, \tag{3.1}$$

$$\theta_r = \frac{\Delta}{1+\Delta}e^{-\left(\frac{1+\Delta}{1+\Delta+\epsilon\Delta}\right)\eta}. \tag{3.2}$$

As suggested by [10], applying quasi linearization to the system of coupled ordinary differential equations (2.7)-(2.8), we have give the following iterative sequences of linear equations

$$a_{0r}f'''_{r+1} + a_{1r}f''_{r+1} + a_{2r}f'_{r+1} + a_{3r}f_{r+1} + a_{4r}\theta'_{r+1} + a_{5r}\theta_{r+1} = R_1, \tag{3.3}$$

$$b_{0r}\theta''_{r+1} + b_{1r}\theta'_{r+1} + b_{2r}\theta_{r+1} + b_{3r}f''_{r+1} + b_{4r}f'_{r+1} + b_{5r}f_{r+1} = R_2, \tag{3.4}$$

where the terms containing subscripts $r+1$ denote present approximations and those containing subscripts r denote previous approximations. The matching boundary conditions are:

$$f_{r+1}(0) = 0, \qquad f'_{r+1}(0) = 1 + \lambda e^{-\gamma\theta_{r+1}}f''_{r+1} + \lambda\alpha f''_{r+1}(0) - \frac{1}{3}\lambda\alpha\delta f''^3_{r+1}(0), \quad \theta'_{r+1}(0) = -\Delta\frac{(1-\theta_{r+1}(0))}{(1+\epsilon\theta_{r+1}(0))}, \tag{3.5}$$

$$f'_{r+1}(\eta) \to 0, \quad \theta_{r+1}(\eta) \to 0 \ \text{ as } \ \eta \to \infty. \tag{3.6}$$

The coefficient parameters $a_{kr}, b_{ir}(k = 0, ..., 4, l = 0, ..., 5), R_1$ and R_2 are defined as

$$R_1 = a_{0r}f'''_r + a_{1r}f''_r + a_{2r}f'_r + a_{3r}f_r + a_{4r}\theta'_r + a_{5r}\theta_r - F_r, \tag{3.7}$$

$$R_2 = b_{0r}\theta''_r + b_{1r}\theta'_r + b_{2r}\theta_r + b_{3r}f''_r + b_{4r}f'_r + b_{5r}f_r - G_r, \tag{3.8}$$

$$F_r = f'''_r(e^{-\gamma\theta_r} + \alpha(1 - \delta f'^2_r)) - \gamma f''_r e^{-\gamma\theta_r}\theta'_r - f'^2_r + f_r f''_r - Mf'_r + G_{rx}\theta_r, \tag{3.9}$$

$$G_r = \frac{1}{Pr}\left((1+\epsilon\theta_r)\theta''_r + \epsilon\theta'^2_r\right) + f_r\theta'_r - 2f'_r\theta_r + Ecf''^2_r\left((e^{-\gamma\theta_r} + \alpha) - \frac{\alpha\delta}{3}f''^2_r\right) + Q\theta_r + MEcf'^2_r + \frac{1}{Pr}R_d\theta''_r, \tag{3.10}$$

$$a_{0r} = \left(e^{-\gamma\theta_r} + \alpha(1 - \delta f'^2_r)\right), \quad a_{1r} = -2\alpha\delta f'''_r f''_r - \gamma e^{-\gamma\theta_r}\theta'_r + f_r, \quad a_{2r} = -2f'_r - M, \tag{3.11}$$

$$a_{3r} = f''_r, \quad a_{4r} = -\gamma f''_r e^{-\gamma\theta}, \quad a_{5r} = -\gamma f'''_r e^{-\gamma\theta} + \gamma^2 f''_r e^{-\gamma\theta}\theta' + G_{rt}, \tag{3.12}$$

$$b_{0r} = \frac{1}{P_r}(1 + \epsilon\theta_r) + \frac{R_d}{P_r}, \quad b_{1r} = \frac{2\epsilon\theta'_r}{P_r} + f_r, \quad b_{2r} = \frac{\epsilon\theta''_r}{P_r} - 2f' - \gamma Ecf''^2_r e^{-\gamma\theta_r} + Q, \tag{3.13}$$

$$b_{3r} = 2Ec(e^{-\gamma\theta} + \alpha)f''_r - \frac{4\alpha\delta Ec}{3}f''^3_r, \quad b_{4r} = -2\theta_r + 2MEcf'_r, \quad b_{5r} = \theta'_r. \tag{3.14}$$

Equations (3.3)-(3.4) are integrated using the Chebyshev spectral collocation method. The boundary condition $[0, \infty)$ is converted to $[-1, 1]$ using the domain transformation $\epsilon = 2\eta/L - 1$ where L is the scaling parameter assumed to be large and the interval $[0, \infty)$ is replaced by $[0, L]$. The Chebyshev nodes in $[-1, 1]$ are defined by the Gauss-Lobatto collocation points[3], [5] given by

$$\epsilon_j = \cos\frac{\pi j}{N}, \qquad \epsilon \in [-1, 1]; \quad j = 0, 1, 2, 3, ..., N. \tag{3.15}$$

The coupled equations (3.3)–(3.5) can then be written in matrix form (3.16). The differentiation matrix used to approximate the derivatives of unknown variables is expressed as $D = 2D/L$, where D is the Chebyshev spectral differentiation matrix of order $(N+1)\times(N+1)$,

$$\begin{bmatrix} A_{11} & A_{12} \\ A_{21} & A_{22} \end{bmatrix} \begin{bmatrix} Y_1 \\ Y_2 \end{bmatrix} = \begin{bmatrix} B_1 \\ B_2 \end{bmatrix}, \tag{3.16}$$

subject to

$$f_{r+1}(\epsilon_{N_\infty}) = 0, \qquad f'_{r+1}(\epsilon_{N_\infty}) = 1 + \lambda e^{-\gamma\theta_{r+1}} f''_{r+1}(\epsilon_{N_\infty}) + \lambda\alpha f''_{r+1}(\epsilon_{N_\infty}) - \frac{1}{3}\lambda\alpha\delta f''^3_{r+1}(\epsilon_{N_\infty}) \tag{3.17}$$

$$\theta'_{r+1}(\epsilon_{N_\infty}) = -\Delta\frac{(1-\theta(\epsilon_{N_\infty}))}{(1+\epsilon\theta(\epsilon_{N_\infty}))}, \tag{3.18}$$

$$f'_{r+1}(\epsilon_{N_0}) = 0 \qquad \theta_{r+1}(\epsilon_{N_0}) = 0. \tag{3.19}$$

In equation (3.16), matrix A has dimension $2(N+1)\times 2(N+1)$, matrices Y and B have dimensions $4(N+1)\times 1$ define in (3.20)-(3.26):

$$A = \begin{bmatrix} A_{11} & A_{12} \\ A_{21} & A_{22} \end{bmatrix}, \tag{3.20}$$

$$A_{11} = a_{0r}D^3 f_{r+1}(\epsilon_j) + a_{1r}D^2 f_{r+1}(\epsilon_j) + a_{2r}Df_{r+1}(\epsilon_j) + a_{3r}f_{r+1}(\epsilon_j)I, \tag{3.21}$$

$$A_{12} = a_{4r}D\theta_{r+1}(\epsilon_j) + a_{5r}\theta_{r+1}(\epsilon_j)I, \tag{3.22}$$

$$A_{21} = b_{3r}D^2 f_{r+1}(\epsilon_j) + b_{4r}Df_{r+1}(\epsilon_j) + b_{5r}f_{r+1}(\epsilon_j)I, \tag{3.23}$$

$$A_{22} = b_{0r}D^2\theta_{r+1}(\epsilon_j) + b_{1r}D\theta_{r+1}(\epsilon_j) + b_{2r}\theta_{r+1}(\epsilon_j)I, \tag{3.24}$$

$$Y = [f_{r+1}(\epsilon_0), f_{r+1}(\epsilon_1), \cdots, f_{r+1}(\epsilon_N), \theta_{r+1}(\epsilon_0), \theta_{r+1}(\epsilon_1), \cdots, \theta_{r+1}(\epsilon_N)]^T, \tag{3.25}$$

$$B = [R_1(\eta_0), R_1(\eta_1), \cdots, R_1(\eta_N), R_2(\eta_0), R_2(\eta_1), \cdots R_2(\eta_N)]^T. \tag{3.26}$$

In the above definitions T stands for transpose, I is an $(N+1)\times(N+1)$ identity matrix and a_{kr} and b_{kr}, $(k = 0, 1, \cdots, n), (r = 0, 1, \cdots, N)$ are diagonal matrices of size $(N+1)\times(N+1)$. After modifying the matrix system in equation (3.16) to incorporate the boundary conditions (3.17)-(3.19), the solution is obtained as

$$Y = A^{-1}B \tag{3.27}$$

4. Outcomes and Discussion

Here, the result of the numerical solutions obtained from the Spectral Quasi Linearization Method (SQLM) are analyzed. To provide a physical insight into the flow problem, pictorial and tabular representations are presented and discussed. The variables are assigned the following values

$$\begin{cases} \alpha = 0.3,\ \delta = 0.3,\ \gamma = 0.1,\ M = 0.2,\ \lambda = 0.2,\ Ec = 0.2, \\ Pr = 1.5,\ \epsilon = 0.2,\ R_d = 0.5,\ Q = 0.1,\ G_{rt} = 0.5, \end{cases}$$

unless otherwise stated.

By setting several fluid parameters to zero, as indicated in Table 1, the present study was cross-referenced with related works found in the literature. The numerical results obtained in Table 1 were compared with the work of Abbas et al. [19], who used the Runge-Kutta method of order four in conjunction with the shooting method, and with that of Hayat et al. [20], who employed the homotopy analysis method. The outcomes of the comparison show excellent agreement with these past works.

The relationship between the Powell-Eyring parameter (α) and the velocity ($f'(\eta)$) and temperature ($\theta(\eta)$) fields is schematically illustrated in Figure 2. Increasing the value of α results in a significant improvement in the velocity distribution and a slight reduction in the temperature distribution. Physically, due to its reciprocal relationship with fluid viscosity, an increase in α causes a rise in fluid velocity.

Fluid viscosity decreases with increasing α , which reduces internal resistance. This allows the fluid molecules to move more freely, leading to a noticeable increase in velocity.

The velocity distribution $(f'(\eta))$ and temperature distribution $(\theta(\eta))$ predictions for the Powell-Eyring parameter (δ) are shown in Fig. 3. It is evident that increasing the numerical value of the δ can somewhat slow down the Powell-Eyring fluid flow, while increasing the value of δ has the opposite effect on the temperature distribution.

The viscosity γ of the Powell-Eyring fluid and its impact on flow $(f'(\eta))$ and the heat transfer mechanism $(\theta(\eta))$ are shown in Figure 4. It is evident that increasing the values of γ reduces fluid velocity, as they are associated with a higher shear stress of Powell-Eyring fluid, which increases the fluid's viscosity. At higher viscosities, the fluid's molecules interact more strongly hindering the fluid's ability to move freely. This increased internal resistance results in a slight decrease in the fluid's overall speed, as the fluid particles encounter greater resistance while flowing. However, the viscosity parameter slightly raises the temperature field, as shown in Fig. 4b.

The impact of the surface-convection parameter (Δ) on the temperature $(\theta(\eta))$ and velocity distributions $f'(\eta)$ is shown in Figure 5. A high value of Δ results in an iincrease in both the fluid temperature and the sheet temperature $\theta(0)$, due to the direct relationship between the surface-convection parameter and the heat transfer coefficient. Furthermore, as the value of Δ increases, the velocity distribution of the boundary layer substantially increases. By physically enhancing the heat exchange at the fluid's surface, the surface-convection parameter promotes a faster transfer of heat from the fluid to its surroundings. As the surface-convection parameter increases, the enhanced heat transfer leads to a rise in the fluid's temperature.

As shown in Figure 6, the influence of the magnetic field's (M) on Powell-Eyring fluid flow within the boundary layer can be utilised to control the velocity field $f'(\eta)$ and generate heat $(\theta(\eta))$. The generation of an increased resistance force known as the Lorentz force, is directly related to increasing values of M and acts perpendicular to the direction of fluid flow. Consequently, as the Lorentz force increases, the impedance force also increases, opposing the fluid flow and thinning the boundary layer. It is evident that increasing the value of M enhances both the temperature distribution and the sheet temperature $\theta(0)$ causing the thickness of the thermal boundary layer to rise as a result.

Figure 7 displays the response of the temperature $(\theta(\eta))$ and velocity profiles $f'(\eta)$ to varying values of thermal conductivity parameter ϵ. There is a slight increase in the fluid velocity distribution due to the thermal conductivity parameter's indirect effect on the fluid velocity field. Additionally, a higher ϵ indicates that the kinetic energy of the molecules is greater. This results in more frequent molecular collisions and, consequently, a higher temperature distribution in the thermal region away from the sheet.

Figure 8 illustrates the changes in the temperature $(\theta(\eta))$ and velocity distributions $f'(\eta)$ as the Eckert number (Ec) varies. The Ec represents the process by which kinetic energy is converted into stored energy and subsequently dissipated as heat when work is done against the stresses of a viscous fluid's. As a result, while the velocity distribution showed a slight increase, a rise in Ec significantly enhances the temperature distribution and sheet temperature $\theta(0)$.

The impact of thermal Grashof number G_{rt} on the flow $(f'(\eta))$ and the heat transfer mechanism $(\theta(\eta))$ is depicted in Figure 9. It is evident that increasing the values of G_{rt} enhances the fluid velocity. This can be attributed to the dominant effect of the buoyancy force when compared to the viscous force acting on the fluid. However, the G_{rt} reduces the temperature field, as shown in Fig. 9b.

The relationship between the Prandtl number (Pr) and the velocity $(f'(\eta))$ and temperature $(\theta(\eta))$ fields is schematically illustrated in Figure 10. An increase Pr results in a decline in both the velocity

distribution and the temperature distribution. This indicates that the effect of thermal diffusivity on the fluid velocity and temperature is greater than that of momentum diffusivity.

The influence of the radiation parameter (R_d) on the Powell-Eyring fluid velocity field ($f'(\eta)$) , and temperature distribution ($\theta(\eta)$) is illustrated in Figure 11. The chart shows an increase in both the fluid velocity and the temperature profile as the radiation parameter increases. An enhanced R_d implies a rise in the kinetic energy of the molecules due to heat. This results in more frequent molecular collisions and, consequently, a higher temperature distribution in the thermal region away from the sheet.

Figure 12 demonstrates the effect of the heat generation/absorption parameter (Q) on the flow profile and the temperature distribution $\theta(\eta)$ of the Powell-Eyring fluid. The Q represents the ratio of the volumetric heat to the density of the fluid at specific heat capacity and constant pressure. As a result, both the fluid flow and temperature profiles improve with an increase in the heat generation/absorption parameter.

The relevance of the slip velocity parameter (λ) on the velocity distribution $f'(\eta)$ and heat transfer rate $\theta(\eta)$ is shown in Figure 13. It has been observed that a decrease in the value of the λ reduces both the temperature profile and the velocity profile. This phenomenon can be explained physically by the slip velocity effect, which is thought to represent the presence of roughness on the sheet's surface or indicate the existence of irregularities. As a result, this specific characteristic slows down the fluid velocity in the boundary layer area.

Following the derivation of the skin friction coefficients $\left(CfRe_x^{\frac{1}{2}}\right)$ and Nusselt number $\left(Nu_xRe_x^{-\frac{1}{2}}\right)$ for the convectively heated Powell- Erying fluid given in equations (2.14) and (2.15), Table 2 highlights the influence of various fluid physical parameters such as Powell-Eyring parameters (α)&(δ), viscosity (γ), magnetic field (M), slip velocity parameter (λ), Eckert number (Ec) , Prandtl number (Pr) , thermal conductivity parameter (ϵ), surface-convection parameter (Δ), radiation parameter (R_d), heat generation/absorption parameter (Q) , and thermal Grashof number (G_{rt}) on the skin friction and Nusselt number. The computed values in the table reveals that the values of $Re_x^{\frac{1}{2}}Cf$ improves when increasing either $\alpha, M, \epsilon,$ or Pr while elevating $\delta, \gamma, \lambda, Ec, Pr, \Delta, R_d, Q,$ or G_{rt} diminishes the skin friction. Moreover, it is observed that local Nusselt number increases when either $\alpha, \lambda, Ec, Pr, \epsilon, \Delta, R_d$ or G_{rt} is increased . Conversely, an increase in M or Q decreases the local Nusselt number. Further analysis of the table shows that rising values of either δ or γ have little effect on the local Nusselt number.

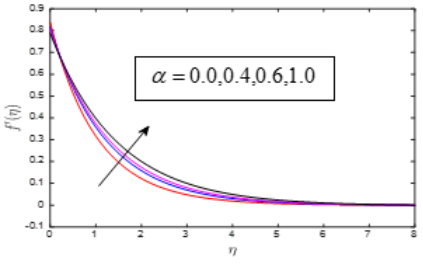

Figure 2a: Effect of α on $f'(\eta)$

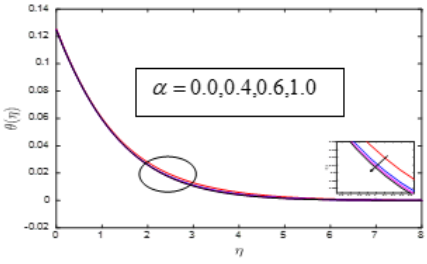

Figure 2b: Effect of α on $\theta(\eta)$

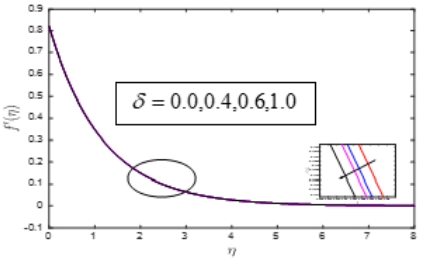

Figure 3a: Effect of δ on $f'(\eta)$

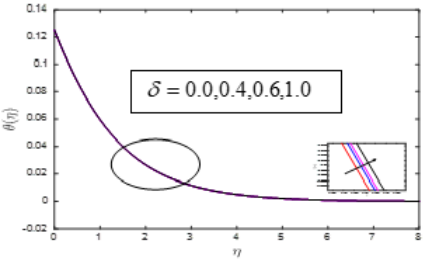

Figure 3b: Effect of δ on $\theta(\eta)$

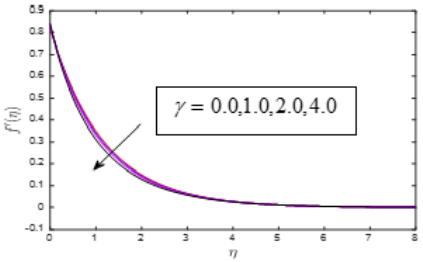

Figure 4a: Effect of γ on $f'(\eta)$

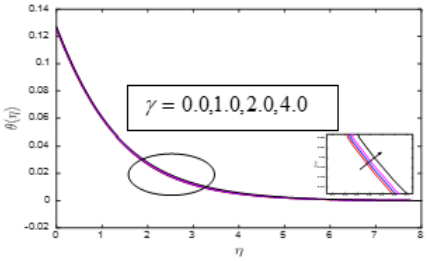

Figure 4b: Effect of γ on $\theta(\eta)$

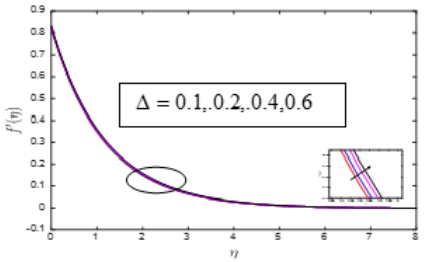

Figure 5a: Effect of Δ on $f'(\eta)$

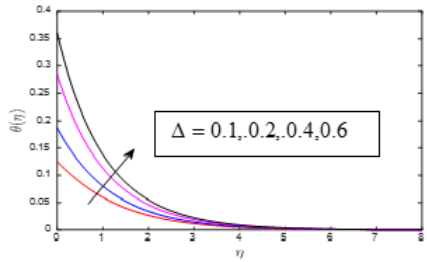

Figure 5b: Effect of Δ on $\theta(\eta)$

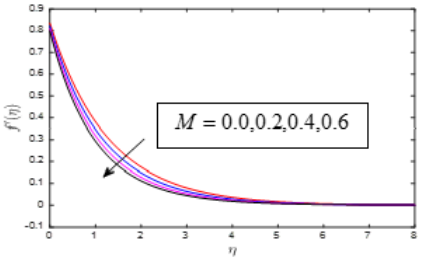

Figure 6a: Effect of M on $f'(\eta)$

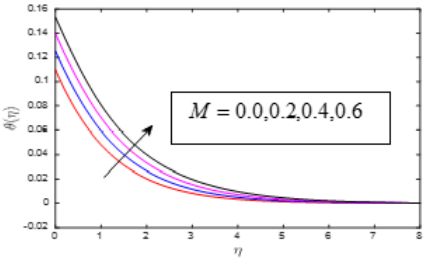

Figure 6b: Effect of M on $\theta(\eta)$

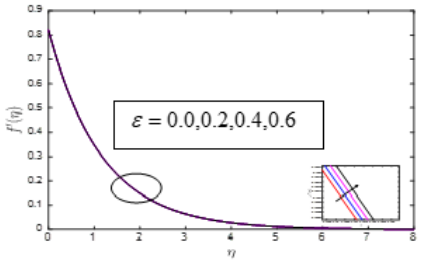

Figure 7a: Effect of ε on $f'(\eta)$

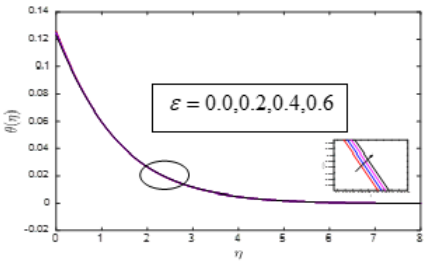

Figure 7b: Effect of ε on $\theta(\eta)$

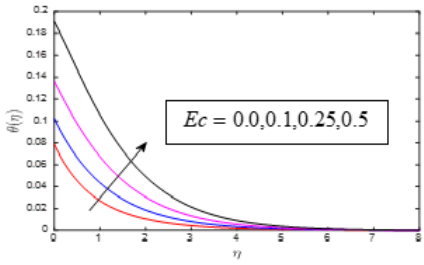

Figure 8a: Effect of Ec on $f'(\eta)$

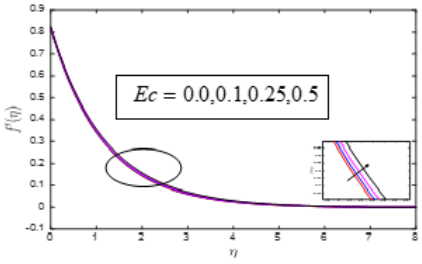

Figure 8b: Effect of Ec on $\theta(\eta)$

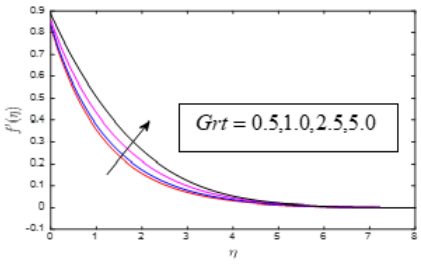

Figure 9a: Effect of G_{rt} on $f'(\eta)$

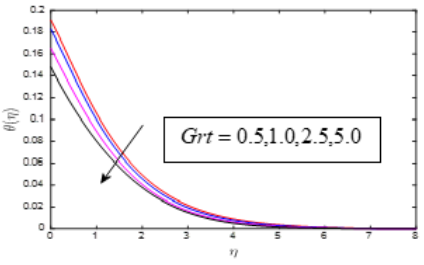

Figure 9b: Effect of G_{rt} on $\theta(\eta)$

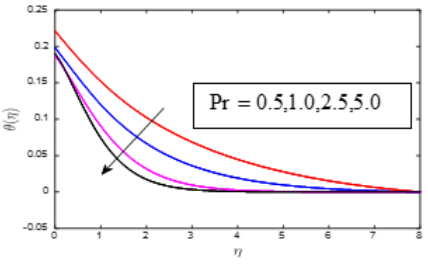

Figure 10a: Effect of $\Pr$ on $f'(\eta)$

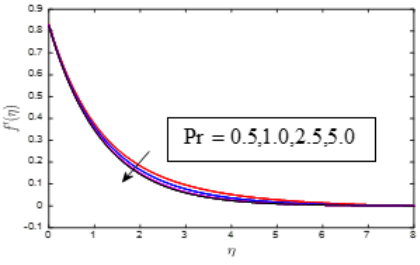

Figure 10b: Effect of $\Pr$ on $\theta(\eta)$

TABLE 1. Table 1: Comparison of $-f''(0)$ for different values of α and δ when $Pr = 1$ and all other fluid variables are to zeros.

α	δ	**Hayat et al**	**Abbass et al**	**Current work**
0.1	0.1	0.956018	0.956016949	0.955420980682675
0.2	0.1	0.917972	0.917971807	0.916012863291598
0.3	0.1	0.883221	0.883219986	0.880935980734648
0.1	0.1	0.956018	0.956016949	0.955420980682675
0.1	0.5	0.964859	0.964858906	0.963183203896961
0.1	0.1	0.975361	0.975310998	0.973574356920722

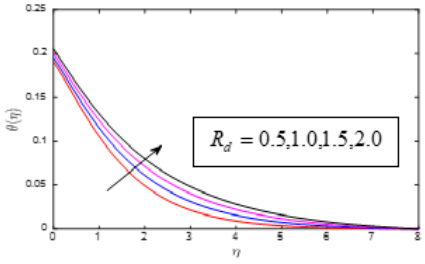

Figure 11a: Effect of R_d on $f'(\eta)$

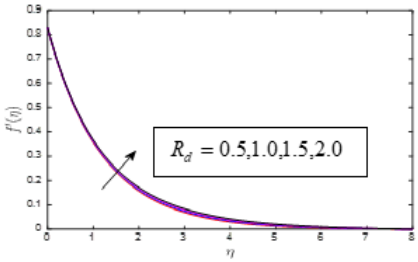

Figure 11b: Effect of R_d on $\theta(\eta)$

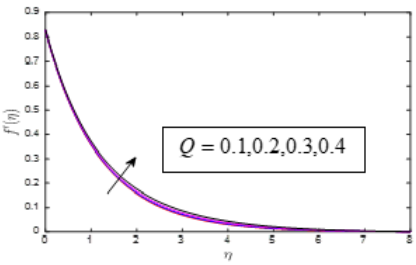

Figure 12a: Effect of Q on $f'(\eta)$

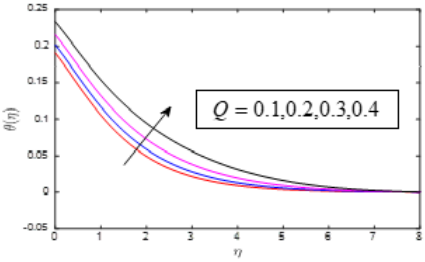

Figure 12b: Effect of Q on $\theta(\eta)$

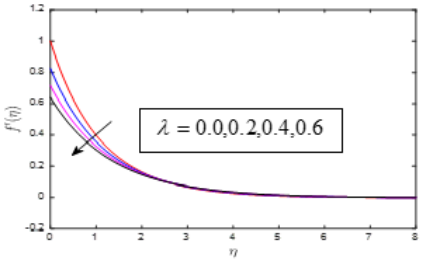

Figure 13a: Effect of λ on $f'(\eta)$

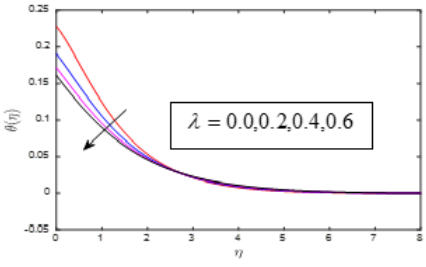

Figure 13b: Effect of λ on $\theta(\eta)$

TABLE 2: Numerical value of $Re_x^{1/2}Cf$ at the surface in the case of shear thickening, shear thinning and Newtonian fluid for various values of De, Re, kp, λ and N_T

α	δ	ε	Δ	λ	M	Pr	Ec	γ	Grt	R_d	Q	$Cf\,\mathrm{Re}_x^{\frac{1}{2}}$	$Nu_x\,\mathrm{Re}_x^{-\frac{1}{2}}$
0.0	0.3	0.2	0.1	0.2	0.2	1.5	0.2	0.1	0.5	0.5	0.1	0.8182	0.1300
0.3	0.3	0.2	0.1	0.2	0.2	1.5	0.2	0.1	0.5	0.5	0.1	0.9050	0.1301
0.3	0.0	0.2	0.1	0.2	0.2	1.5	0.2	0.1	0.5	0.5	0.1	0.9073	0.1301
0.3	0.3	0.2	0.1	0.2	0.2	1.5	0.2	0.1	0.5	0.5	0.1	0.9050	0.1301
0.3	0.3	0.0	0.1	0.2	0.2	1.5	0.2	0.1	0.5	0.5	0.1	0.9050	0.1310
0.3	0.3	0.2	0.1	0.2	0.2	1.5	0.2	0.1	0.5	0.5	0.1	0.9050	0.1301
0.3	0.3	0.2	0.0	0.2	0.2	1.5	0.2	0.1	0.5	0.5	0.1	0.9158	0
0.3	0.3	0.2	0.1	0.2	0.2	1.5	0.2	0.1	0.5	0.5	0.1	0.9050	0.1301
0.3	0.3	0.2	0.1	0.0	0.2	1.5	0.2	0.1	0.5	0.5	0.1	1.2062	0.1282
0.3	0.3	0.2	0.1	0.2	0.2	1.5	0.2	0.1	0.5	0.5	0.1	0.9050	0.1301
0.3	0.3	0.2	0.1	0.2	0.0	1.5	0.2	0.1	0.5	0.5	0.1	0.8355	0.1325
0.3	0.3	0.2	0.1	0.2	0.2	1.5	0.2	0.1	0.5	0.5	0.1	0.9050	0.1301
0.3	0.3	0.2	0.1	0.2	0.2	1.0	0.2	0.1	0.5	0.5	0.1	0.8972	0.1278
0.3	0.3	0.2	0.1	0.2	0.2	1.5	0.2	0.1	0.5	0.5	0.1	0.9050	0.1301
0.3	0.3	0.2	0.1	0.2	0.2	1.5	0.0	0.1	0.5	0.5	0.1	0.9192	0.1375
0.3	0.3	0.2	0.1	0.2	0.2	1.5	0.2	0.1	0.5	0.5	0.1	0.9050	0.1301
0.3	0.3	0.2	0.1	0.2	0.2	1.5	0.2	0.0	0.5	0.5	0.1	0.9022	0.1302
0.3	0.3	0.2	0.1	0.2	0.2	1.5	0.2	0.1	0.5	0.5	0.1	0.9050	0.1301
0.3	0.3	0.2	0.1	0.2	0.2	1.5	0.2	0.1	0.0	0.5	0.1	0.9341	0.1296
0.3	0.3	0.2	0.1	0.2	0.2	1.5	0.2	0.1	0.5	0.5	0.1	0.9050	0.1301
0.3	0.3	0.2	0.1	0.2	0.2	1.5	0.2	0.1	0.5	0.2	0.1	0.9082	0.1053
0.3	0.3	0.2	0.1	0.2	0.2	1.5	0.2	0.1	0.5	0.5	0.1	0.9050	0.1301
0.3	0.3	0.2	0.1	0.2	0.2	1.5	0.2	0.1	0.5	0.5	0.0	0.9075	0.1311
0.3	0.3	0.2	0.1	0.2	0.2	1.5	0.2	0.1	0.5	0.5	0.1	0.9050	0.1301

5. CONCLUSION

The MHD flow of an Erying-Powell fluid over a convectively heated stretched sheet with convective boundary conditions has been solved using the Spectral Quasi-Linearization Method (SQLM). The summary of the analyses in this research work is outlined as follows:

(i) The slip velocity parameter reduces the skin friction coefficient, temperature distribution, and velocity profile but increases the Nusselt number.
(ii) The surface-convection parameter increases the fluid velocity, fluid temperature, sheet temperature, and Nusselt number but reduces the skin friction coefficient.
(iii) The magnetic field parameter enhances both the sheet temperature and temperature distribution while reducing the fluid flow and Nusselt number.
(iv) Both the fluid flow and temperature profiles improve with an increase in the heat generation/absorption parameter, but the opposite is true for the skin friction coefficient and Nusselt number.

(v) The skin friction coefficient decreases with an increase in either the radiation parameter or the Eckert number. However, the fluid velocity, temperature profile, and Nusselt number increase with an increase in the radiation parameter or the Eckert number.

(vi) As the thermal Grashof number increases, the fluid velocity and Nusselt number improve, while the temperature profile and skin friction coefficient decrease.

6. Limitations of the Present Study

This study focused on a limited scope of fluid variables, including viscous dissipation, Joule heating, a uniform magnetic field, thermal radiation, temperature-dependent viscosity and thermal conductivity, and a heat source, to analyze the flow of an Eyring-Powell fluid under velocity slip and convective boundary conditions.

7. Suggestions for Future Works

The current study can be expanded to explore the unsteady flow of Eyring-Powell fluids, incorporating a non-uniform magnetic field, Cattaneo-Christov heat flux models, and mixed or radiative boundary conditions along different geometries. Additionally, entropy analysis could be integrated into the model to assess thermodynamic efficiency. A suitable closed-form or semi-analytical solution to the problem can be attempted, and the results could be validated using a numerical method to ensure accuracy and reliability.

References

[1] W. Abbas, , M. M. Ahmed, *Powell-Eyring fuid fow over a stratifed sheet through porous medium with thermal radiation and viscous dissipation.* AIMS Math. **6**(2021), 13464–13479.

[2] W. Abbas, M. M. Ahmed, M. S. Emam, Hassan M. H. Sadek, *MHD dissipative Powell Eyring fluid flow due to a stretching sheet with convective boundary conditions and slip velocity.* Scientific Reports, **13**(2023): 15674. https://doi.org/10.1038/s41598-023-42609-w

[3] M. N. Asimoni, N. F. Mohammad, A. M. Kasim, S. Shafie, *MHD mixed convective flow of power-law nanofluid in a lid-driven cavity with heat generation and chemical reaction effects: buongiorno's Model.* Malaysian J Fund Appl Sci. **16(5)**(2020), 576– 84.

[4] K. K. Asogwa, S. M. Bilal, I. L. Animasaun, and F. M. Mebarek-Oudina. *Insight into the significance of ramped wall temperature and ramped surface concentration: The case of Casson fluid flow on an inclined Riga plate with heat absorption and chemical reaction. Nonlinear Engineering* **(10)**(2021), 213–230.

[5] I. Athal, B. Haewon, A. Sasikala, B. Narsimha Reddy, V. Govindan, P. Maddileti, & R. Mishra, *Combined impact of radiation and chemical reaction on MHD hyperbolic tangent nanofluid boundary layer flow past a stretching sheet,* Modern Physics Letters B, **38(16)**(2024): 2341010.

[6] H. A. Attia, W. Abbas, A. L. Aboul-Hassan, M. A. M.Abdeen, M. A. Ibrahim, *Unsteady flow of a dusty Bingham fluid through a porous medium in a circular pipe.* J. Appl. Mech. Tech. Phys. **57**(2016), 596–602.

[7] M. Bilal, M. Sagheer, S. Hussain, *Numerical study of magnetohydrodynamic and thermal radiation on Williamson nanofluid flow over a stretching cylinder with variable thermal conductivity,* Alex. Eng. J. **57**(2018), 3281–3289.

[8] A. J. Chamkha, A. A. Khaled, *Similarity solutions for hydromagnetic simultaneous heat and mass transfer by natural convection from an inclined plate with heat generation or absorption.* Heat Mass Transf. **37(2-3)**(2001), 117–23.

[9] A. J. Chamkha, Aly, A. M. Mansour, *Similarity solution for unsteady heat and mass transfer from a stretching surface embedded in a porous medium with suction/injection and chemical reaction efects.* Chem. Eng. Commun. **197**(2010), 846–858.

[10] A. J. Chamkha, *Unsteady MHD convective heat and mass transfer past a semi-infinite vertical permeable moving plate with heat absorption.* Int J Eng Sci. **42(2)**(2004), 217–30.

[11] L.J. Crane, *Flow past a stretching plate.* Z. Angew, Math. Phys. **21**(1970), 645–647.

[12] Y S Daniel, Z A Aziz, Z Ismail and F Salah, *Thermal radiation on unsteady electrical MHD flow of nanofluid over stretching sheet with chemical reaction* J. King Saud University– Sci. **31**(2019): 804.

[13] T. Hayat, M. Awais, S. Asghar, *Radiative efects in a three-dimensional fow of MHD Eyring-Powell fuid.* J. Egypt. Math. Soc. **21**(2013), 379–384.

[14] T. Hayat, S. Nadeem,*Flow of 3D Eyring-Powell fluid by utilizing Cattaneo-Christov heat flux model and chemical processes over an exponentially stretching surface.*Results Phys. **8**(2018), 397–403.

[15] T. Hayat, Z. Iqbal, M. Qasim, S. Obidat, *Steady flow of an Eyring Powell fluid over a moving surface with convective boundary conditions,* Int. J. Heat Mass Transf. **55**(2012), 1817– 1822.

[16] W. Ibrahim, B. Shankar, M.M. Nandeppanavar, *MHD stagnation point flow and heat transfer due to nanofluid towards a stretching sheet,* Int. J. Heat Mass Transf. **56**(2013), 1–9.

[17] P. G. Janthe, J. V. Tawade, H. A. Mahmoud, M. El-Meligy,& M. I. Khan. *Thin film flows on a linearly moving surface with thermocapillary effects and variable heat generation/absorption.* Journal of Radiation Research and Applied Sciences, **17(4)**(2024): 101135.

[18] M. M. Khader, M. M. Babatin, *Numerical study for improvement the cooling process through a model of Powell-Eyring fluid flow over a stratified stretching sheet with magnetic field.* Case Stud. Term. Eng. **31**(2022): 101786.

[19] K. T. Kumar, S. Kalyan, M. Kandagal, J. V. Tawade, U. Khan , S. M. Eldin, & A. M. Abed. *Influence of heat generation/absorption on mixed convection flow field with porous matrix in a vertical channel.* Case Studies in Thermal Engineering **47**(2023): 103049.

[20] M. Kumari, G. Nath, *Flow and heat transfer in a stagnation-point flow over a stretching sheet with a magnetic field.* Mech. Res. Commun. **26**(1999), 469–478.

[21] A. López, G. Ibáñez, J. P. Enríquez, J. Moreira, O. Lastres, *Entropy generation analysis of MHD nanofluid flow in a porous vertical microchannel with nonlinear thermal radiation, slip flow and convective-radiative boundary conditions,* Int. J. Heat Mass Tran. **107**(2017), 982–994.

[22] B. K. Manvi, S. B. Kerur, J. V. Tawade, J. J. Nieto, S. N. Sankeshwari, H. Ahmad, & V. Govindan, MHD *Casson nanofluid boundary layer flow in presence of radiation and non-uniform heat source/sin,* Model. Control, **3**(2023), 152-167.

[23] B. Manvi, J. Tawade, M. Biradar, S. Noeiaghdam, U. Fernandez-Gamiz, & V. Govindan. *The effects of MHD radiating and non-uniform heat source/sink with heating on the momentum and heat transfer of Eyring-Powell fluid over a stretching. Results in Engineering,* **14**(2022): 100435.

[24] A. M. Megahed, W. Abbas, *Non-Newtonian Cross fluid flow through a porous medium with regard to the efect of chemical reaction and thermal stratification phenomenon.* Case Stud. Term. Eng. **29**(2022): 101715.

[25] A S Mittal and H R Patel, *Influence of thermophoresis and Brownian motion on mixed convection two dimensional MHD Casson fluid flow with non-linear radiation and heat generation,* Physica A **537**(2020): 122710.

[26] S. Mukhopadhyay, *Slip effects on MHD boundary layer flow over an exponentially stretching sheet with suction/blowing and thermal radiation,* Ain Shams Eng. J. **4**(2013), 485–491.

[27] M. E. Nasr, *Analysis of non-linear radiation and activation energy analysis on hydromagnetic Reiner-Philippof fluid flow with Cattaneo-Christov double diffusions.* Mathematics **10**(2022): 1534.

[28] S. Panigrahi, M. Reza, A. K. Mishra, *Mixed convective fow of a Powell-Eyring fluid over a non-linear stretching surface with thermal diffusion and diffusion thermo.* Procedia Eng. **127**(2015), 645–651.

[29] M. Patel, M.G. Timol, *Numerical treatment of Powell-Eyring fluid flow using method of satisfaction of asymptotic boundary conditions (MSABC)*, Appl. Numer. Math. **59**(2009), 2584– 2592.

[30] A.M. Rashad, *Impact of thermal radiation on MHD slip flow of ferrofluid over a non-isothermal wedge,* J. Magn. Magn Mater. **422**(2017), 25–31.

[31] A.V. Rosca, I.M. Pop, *Flow and heat transfer of Powell-Eyring fluid over a shrinking surface in a parallel free stream,* Int. J. Heat Mass Transf. **71**(2014), 321–327.

[32] K Sharma, *FHD flow and heat transfer over a porous rotating disk accounting for Coriolis force along with viscous dissipation and thermal radiation,* Heat Transfer **51(5)** (2022): 4377.

[33] J. V. Tawade, *Efects of thermophoresis and Brownian motion for thermal and chemically reacting Casson nanofuid flow over a linearly stretching sheet.* Results Eng. **15** (2022): 100448.

[34] M. Turkyilmazoglu, *Exact solutions for two-dimensional laminar flow over a continuously stretching or shrinking sheet in an electrically conducting quiescent couple stress fluid.* Int. J. Heat Mass Transf. **72** (2014), 1–8.

L.O. Sogbetun, corresponding author, Department of Mathematics, Federal University of Agriculture, Abeokuta, Nigeria
Email address: sogbetunlateef@gmail.com

Department of Mathematics, Federal University of Agriculture, Abeokuta, Nigeria
Email address: ishola1@gmail.com

Department of Mathematics, Federal University of Agriculture, Abeokuta, Nigeria
Email address: fagbemiroo@funaab.edu.ng